nature medicine

Targeting focal adhesion kinase renders pancreatic cancers responsive to checkpoint immunotherapy

Hong Jiang[1,2], Samarth Hegde[1,2], Brett L Knolhoff[1,2], Yu Zhu[1,2], John M Herndon[1,2], Melissa A Meyer[1,2], Timothy M Nywening[3], William G Hawkins[3,4], Irina M Shapiro[5], David T Weaver[5], Jonathan A Pachter[5], Andrea Wang-Gillam[1,4] & David G DeNardo[1,2,4,6]

Single-agent immunotherapy has achieved limited clinical benefit to date in patients with pancreatic ductal adenocarcinoma (PDAC). This may be a result of the presence of a uniquely immunosuppressive tumor microenvironment (TME). Critical obstacles to immunotherapy in PDAC tumors include a high number of tumor-associated immunosuppressive cells and a uniquely desmoplastic stroma that functions as a barrier to T cell infiltration. We identified hyperactivated focal adhesion kinase (FAK) activity in neoplastic PDAC cells as an important regulator of the fibrotic and immunosuppressive TME. We found that FAK activity was elevated in human PDAC tissues and correlated with high levels of fibrosis and poor $CD8^+$ cytotoxic T cell infiltration. Single-agent FAK inhibition using the selective FAK inhibitor VS-4718 substantially limited tumor progression, resulting in a doubling of survival in the *p48-Cre*;*LSL-Kras*^{G12D};*Trp53*$^{flox/+}$ (KPC) mouse model of human PDAC. This delay in tumor progression was associated with markedly reduced tumor fibrosis and decreased numbers of tumor-infiltrating immunosuppressive cells. We also found that FAK inhibition rendered the previously unresponsive KPC mouse model responsive to T cell immunotherapy and PD-1 antagonists. These data suggest that FAK inhibition increases immune surveillance by overcoming the fibrotic and immunosuppressive PDAC TME and renders tumors responsive to immunotherapy.

The application of immunotherapy holds great promise for improving pancreatic cancer patient outcomes, as it has already done for patients with melanoma or lung cancer. Unfortunately, to date, attempts at immunotherapy in PDAC have achieved limited clinical benefits when deployed as single agents[1]. This is likely a result in part of the presence of a uniquely immunosuppressive TME that is dominant in most human PDACs. This immunosuppressive TME is an important regulator of disease progression and poor responses to conventional therapy. Major drivers of this pro-tumorigenic microenvironment include a highly fibrotic stroma and extensive infiltration by immunosuppressive cell populations[2–7]. High stromal density can provide a barrier to the delivery of cytotoxic agents and has been postulated to limit T cell access to tumor cells and function once recruited in the tumor site[8–11]. In addition, extensive myeloid cell infiltration, typical of PDAC, may further lead to the dysfunction of PDAC-infiltrating T cells[2,4,6,12,13]. Thus, agents that can overcome excessive fibrosis to alter immune suppression would be particularly attractive therapeutics for PDAC.

FAKs are nonreceptor tyrosine kinases, which include FAK1 and PYK2 (also known as FAK2). Of these, FAK1 has been heavily studied in the context of cancer cell migration, proliferation, and survival (reviewed in refs. 14,15). Several studies have demonstrated that elevated FAK1 expression enhances tumor malignancy and correlates with poor prognosis[14]. More recently, FAK1 has been implicated in regulating pro-inflammatory pathway activation and cytokine production[15,16]. In addition, FAK signaling has been implicated in wound healing and/or pathologic fibrosis in several tissues[17–25]. Because of the role of FAK in translating signals from extracellular matrix composition and/or stiffness into intracellular pro-inflammatory pathway regulation, it seems plausible that FAK might be important for regulating the fibrotic PDAC TME[25]. We sought to determine the effect of FAK signaling in maintaining the fibrotic and immunosuppressive TME of PDAC. We found that FAK1 is a central driver of the fibrotic and immunosuppressive microenvironment that protects tumors from immune surveillance and drives resistance to immunotherapy.

RESULTS

FAK is hyperactivated in human PDAC and correlates with immunosuppressive TMEs

To evaluate whether FAK activation might affect the TME, we analyzed human PDAC tumor tissues for the expression of total and phosphorylated FAK1 (Tyr-397, p-FAK1) and PYK2 (FAK2) by immunohistochemistry (IHC). We found that both total FAK1 and p-FAK1 were upregulated as compared to that in normal pancreatic tissue in 80% (45 of 56) and 84% (47 of 56) of patients, respectively (**Fig. 1a** and

[1]Department of Medicine, Washington University School of Medicine, St. Louis, Missouri, USA. [2]Integrating Communications within the Cancer Environment (ICCE) Institute, Washington University School of Medicine, St. Louis, Missouri, USA. [3]Department of Surgery, Washington University School of Medicine, St. Louis, Missouri, USA. [4]Siteman Cancer Center, Washington University School of Medicine, St. Louis, Missouri, USA. [5]Verastem Inc., Needham, Massachusetts, USA. [6]Department of Pathology and Immunology, Washington University School of Medicine, St. Louis, Missouri, USA. Correspondence should be addressed to D.G.D. (ddenardo@dom.wustl.edu).

Received 5 March; accepted 10 May; published online 4 July 2016; doi:10.1038/nm.4123

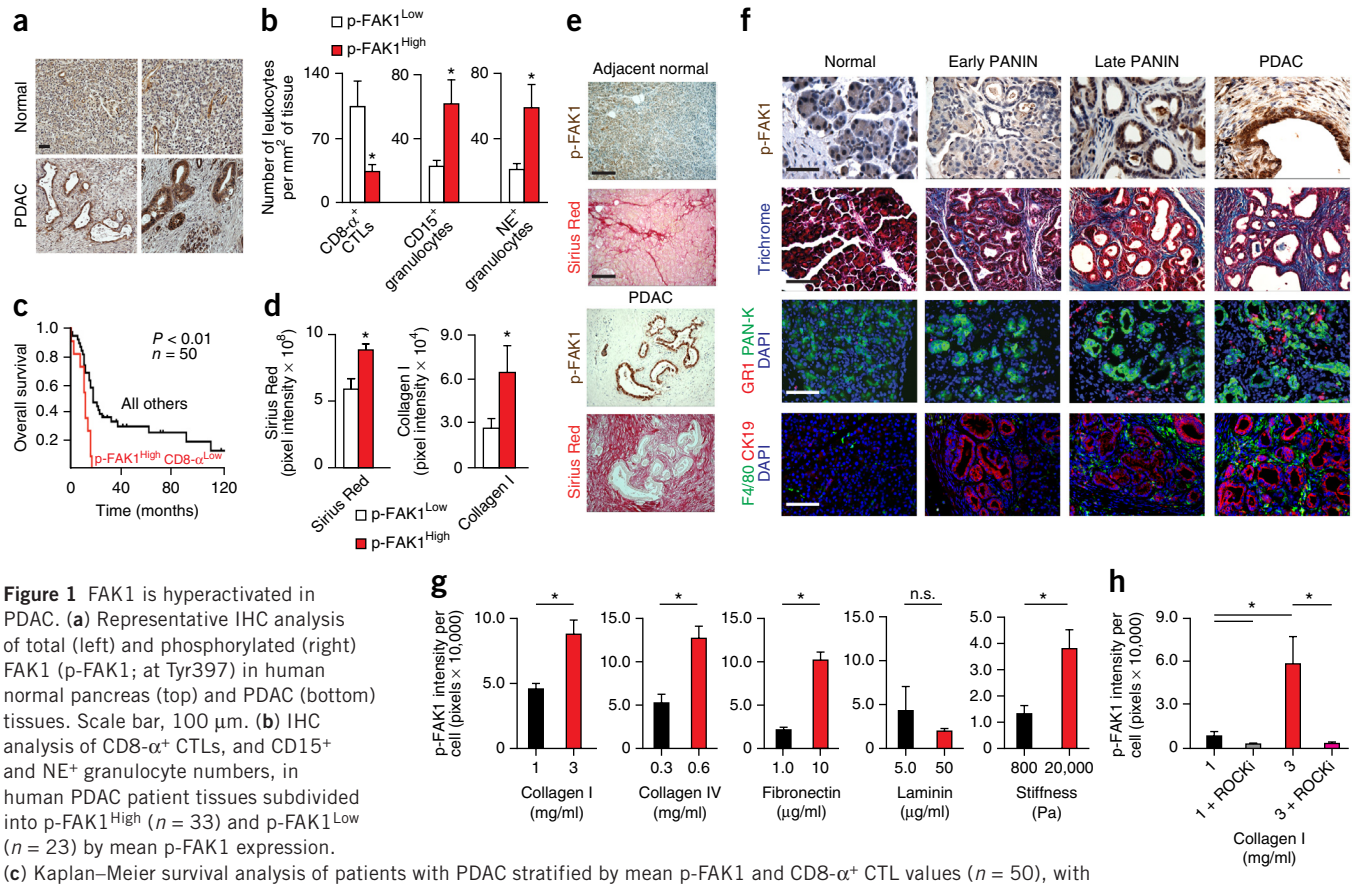

Figure 1 FAK1 is hyperactivated in PDAC. (**a**) Representative IHC analysis of total (left) and phosphorylated (right) FAK1 (p-FAK1; at Tyr397) in human normal pancreas (top) and PDAC (bottom) tissues. Scale bar, 100 μm. (**b**) IHC analysis of CD8-α$^+$ CTLs, and CD15$^+$ and NE$^+$ granulocyte numbers, in human PDAC patient tissues subdivided into p-FAK1^{High} ($n = 33$) and p-FAK1^{Low} ($n = 23$) by mean p-FAK1 expression. (**c**) Kaplan–Meier survival analysis of patients with PDAC stratified by mean p-FAK1 and CD8-α$^+$ CTL values ($n = 50$), with p-FAK1^{High} CD8-α^{Low} group displayed versus all other groups. (**d**) Quantification of Sirius Red staining (total collagen) or collagen I in human PDAC tumor tissues subdivided into p-FAK1^{High} and p-FAK1^{Low} by mean p-FAK1 expression. (**e**) Representative IHC for p-FAK1 and staining for Sirius Red in human PDAC and adjacent 'normal' tissue. Scale bar, 400 μm. (**f**) Representative IHC for p-FAK1, trichrome (total collagen), GR1$^+$ granulocytes and F4/80$^+$ TAMs in normal pancreatic tissue, early PANIN, late PANIN and PDAC tumor from KPC mice. Cytokeratin 19 (CK19) and pan-keratin (PAN-K) mark pancreatic epithelial cells. Scale bars, 100 μm (p-FAK1) and 200 μm (Trichrome, GR-1 and F4/80). (**g**) Immunofluorescence analysis of p-FAK1 expression in KP cells cultured on collagen I gel, collagen IV–coated plates, fibronectin (FN1)-coated or laminin-coated polyacrylamide gels, and FN1-coated compliant (800 Pa)/rigid (20 kPa) polyacrylamide gels. (**h**) Immunofluorescence analysis of p-FAK1 expression in KP cells cultured on collagen I gel and treated with vehicle or ROCKi (Y-27632). Error bars represent mean ± s.e.m.; $^*P < 0.05$; n.s., not significant; by unpaired two-sided Student's *t* test (**b**,**d**,**g**), log-rank test (**c**) or one-way analysis of variance (ANOVA) with Tukey's method for multiple comparisons (**h**).

Supplementary Fig. 1a,**b**). IHC also revealed that, although stromal cells had detectable expression of both total FAK1 and p-FAK1 relative to those in control stains, PDAC neoplastic cells expressed far higher levels of total FAK1 and p-FAK1.

To determine whether high levels of FAK1 activation in PDAC cells correlate with changes in the TME, we stratified human PDAC patients on the basis of high or low epithelial (tumor cell) p-FAK1 levels using mean IHC intensity. We found that high p-FAK1 levels in tumor cells were associated with lower numbers of tumor-infiltrating CD8$^+$ cytotoxic T lymphocytes (CTLs), and higher prevalence of both neutrophil elastase$^+$ (NE$^+$) and CD15$^+$ granulocytes (**Fig. 1b** and **Supplementary Fig. 1c**). On the basis of the inverse correlation between p-FAK levels and tumor infiltration by CD8$^+$ CTLs, we analyzed the association of this with patient survival and found that high p-FAK1 and low CD8$^+$ CTL levels were indicative of poor clinical outcomes (**Fig. 1c** and **Supplementary Fig. 1c**,**d**). To determine how FAK1 activation correlates specifically with tumor fibrosis, we analyzed both total collagen amounts by Sirius Red staining and collagen I, III and IV deposition by IHC. Although the majority of samples showed high levels of fibrosis, we found that tumors with high p-FAK1 expression also had higher levels of total stromal collagen and collagen I deposition (**Fig. 1d**,**e** and **Supplementary Fig. 1e**). We found that the extent of collagen I deposition, but not of collagen III or collagen IV deposition, correlated with the amount of p-FAK expression ($r = 0.299$, $P = 0.028$, $n = 50$). Taken together, these data suggest that high levels of tumor FAK1 activation are indicative of a fibrotic and immunosuppressive TME.

To determine the stage of tumor progression at which FAK1 becomes hyperactivated and how this correlates with changes in the TME, we analyzed p-FAK1 expression in pancreatic tissue from the KPC mouse model (**Fig. 1f**). We found that p-FAK1 was barely detectable in the normal pancreatic epithelium and early pancreatic intraepithelial neoplasia lesions (PanIN). However, p-FAK1 levels were modestly upregulated in late PanINs and substantially elevated in PDAC lesions. The absence of FAK hyperactivation in early-stage PanIN lesions suggests that, in contrast with recent reports in mouse models of lung cancer[26], *Kras*^{G12D} expression alone is not sufficient to induce FAK activation. Consistent with this, we found that neither the overexpression of *Kras*^{G12V} in human pancreatic epithelial cells (PDECs) nor the knockdown of *Kras* in KPC-derived tumor cells (KP cells) led to alterations in total FAK1 or p-FAK1 expression (**Supplementary Fig. 2a**,**b**). In contrast, we found that matrix stiffness

or increased density of collagen I, collagen IV or fibronectin, but not laminin, resulted in elevated FAK activation (**Fig. 1g** and **Supplementary Fig. 2c–f**). We also observed that the induction of p-FAK1 by collagen density was Rho-associated coiled-coil kinase (ROCK) dependent (**Fig. 1h**). These data are also consistent with observations from several other research groups that collagen density or stiffness can lead to FAK activation in other normal and malignant cell types[27–30]. Following analysis of the TME present when FAK1 is hyperactivated in KPC mice, we found that p-FAK1 expression is high in PDAC lesions that have extensive collagen deposition and tumor-infiltration by inflammatory cells (F4/80$^+$ and GR1$^+$), but few CD8$^+$ CTLs (**Fig. 1f** and **Supplementary Fig. 2g**). Together, these findings suggest that FAK activation in tumor cells might play a key role in establishing the immunosuppressive TME.

FAK inhibition leads to temporary tumor stasis and extended survival in KPC mice

To assess the impact of inhibiting FAK on PDAC progression, we evaluated a clinically available dual FAK1 and FAK2 inhibitor, VS-4718 (hereafter referred to as FAKi; **Supplementary Fig. 3a**), in the genetic KPC and *p48-Cre*;*LSL-Kras*^{G12D};*Trp53*$^{flox/flox}$ (KPPC) mouse models. We evaluated both early and late therapeutic strategies by either treating KPC mice at 3.5 months of age, when over 90% of these mice have histological microscopic PDAC lesions (early), or when overt (palpable) and/or ultrasound-detectable (>0.5 cm in diameter) tumors were identified (late). We found that single-agent FAK inhibition caused a significant and similar extension of survival in both early and late treatment groups (**Fig. 2a**). These results are particularly notable in comparison with gemcitabine (GEM) treatment, a standard clinical

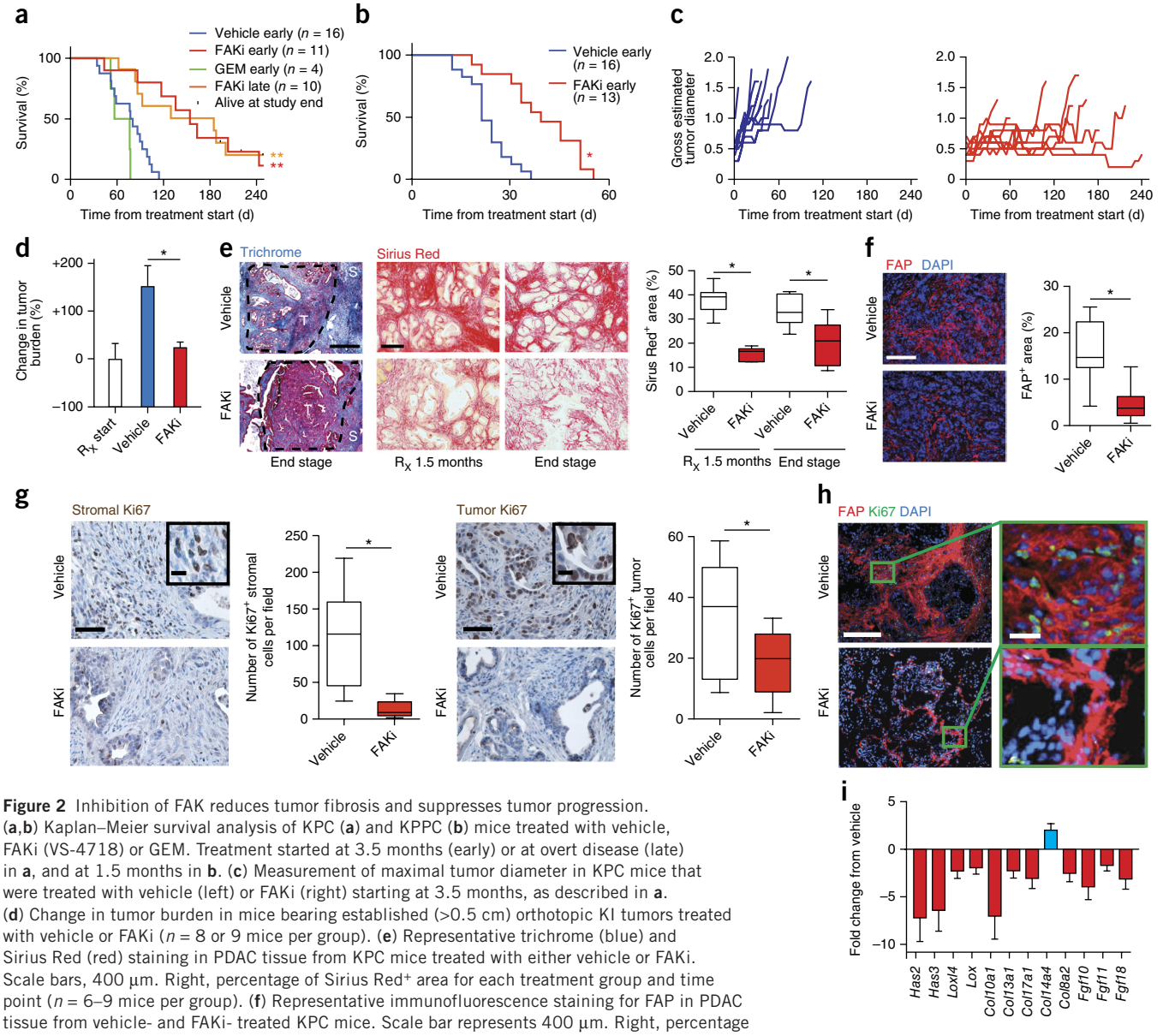

Figure 2 Inhibition of FAK reduces tumor fibrosis and suppresses tumor progression. (**a**,**b**) Kaplan–Meier survival analysis of KPC (**a**) and KPPC (**b**) mice treated with vehicle, FAKi (VS-4718) or GEM. Treatment started at 3.5 months (early) or at overt disease (late) in **a**, and at 1.5 months in **b**. (**c**) Measurement of maximal tumor diameter in KPC mice that were treated with vehicle (left) or FAKi (right) starting at 3.5 months, as described in **a**. (**d**) Change in tumor burden in mice bearing established (>0.5 cm) orthotopic KI tumors treated with vehicle or FAKi ($n = 8$ or 9 mice per group). (**e**) Representative trichrome (blue) and Sirius Red (red) staining in PDAC tissue from KPC mice treated with either vehicle or FAKi. Scale bars, 400 μm. Right, percentage of Sirius Red$^+$ area for each treatment group and time point ($n = 6$–9 mice per group). (**f**) Representative immunofluorescence staining for FAP in PDAC tissue from vehicle- and FAKi- treated KPC mice. Scale bar represents 400 μm. Right, percentage of FAP$^+$ area for each treatment group ($n = 11$–13 mice per group). (**g**) Representative IHC and quantification for stromal and tumor Ki67$^+$ cells from vehicle- and FAKi-treated KPC mice ($n = 8$–11 mice per group). Scale bars represent 200 μm (inset, 50 μm). (**h**) Representative immunofluorescence staining for FAP and Ki67 in PDAC tissue from vehicle- and FAKi-treated KPC mice. Scale bars represent 400 μm (magnified field, 50 μm). (**i**) mRNA expression analysis from gene array of orthotopic KP tumors following 14-d treatment with vehicle or FAKi ($n = 6$ or 7 mice per group). Error bars represent mean ± s.e.m. $^*P < 0.05$, $^{**}P < 0.01$; by log-rank test (**a**,**b**) or unpaired two-sided Student's *t*-test (**d**–**g**).

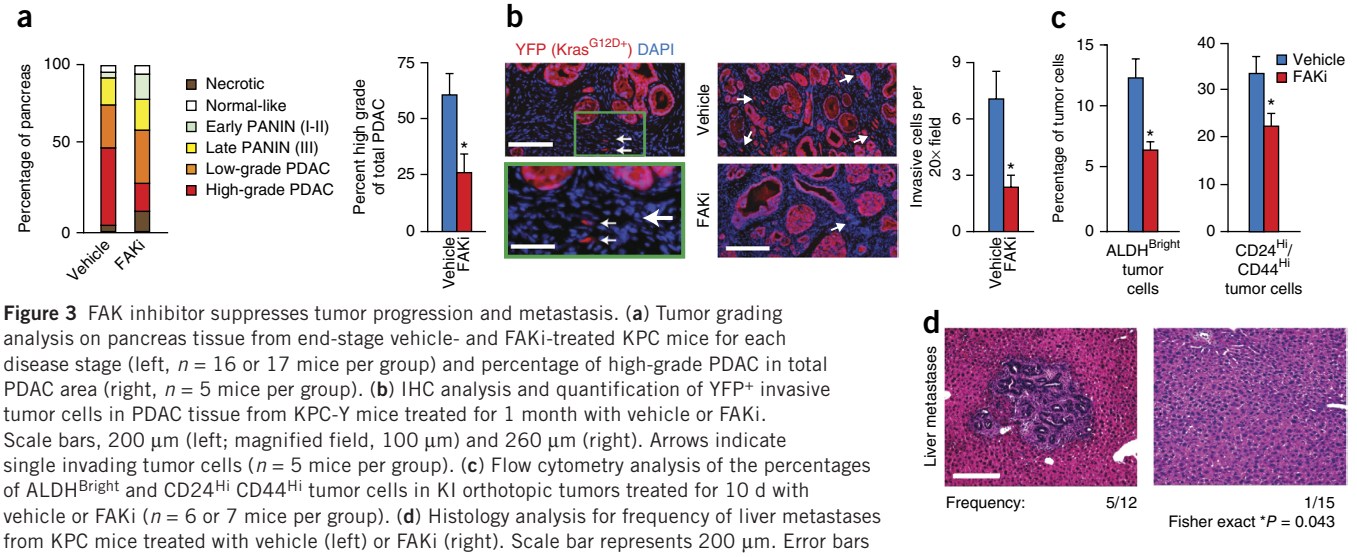

Figure 3 FAK inhibitor suppresses tumor progression and metastasis. (**a**) Tumor grading analysis on pancreas tissue from end-stage vehicle- and FAKi-treated KPC mice for each disease stage (left, $n = 16$ or 17 mice per group) and percentage of high-grade PDAC in total PDAC area (right, $n = 5$ mice per group). (**b**) IHC analysis and quantification of YFP$^+$ invasive tumor cells in PDAC tissue from KPC-Y mice treated for 1 month with vehicle or FAKi. Scale bars, 200 μm (left; magnified field, 100 μm) and 260 μm (right). Arrows indicate single invading tumor cells ($n = 5$ mice per group). (**c**) Flow cytometry analysis of the percentages of ALDH^{Bright} and CD24^{Hi} CD44^{Hi} tumor cells in KI orthotopic tumors treated for 10 d with vehicle or FAKi ($n = 6$ or 7 mice per group). (**d**) Histology analysis for frequency of liver metastases from KPC mice treated with vehicle (left) or FAKi (right). Scale bar represents 200 μm. Error bars represent mean ± s.e.m. *$P < 0.05$; by Student's *t*-test (**a**–**c**) or Fisher's exact test (**d**).

treatment, which has no effect on survival in these models. A similar improvement of survival was observed in the extremely aggressive KPPC mouse model when mice bearing overt PDAC tumors were treated with FAKi (**Fig. 2b**). To assess whether single-agent FAK inhibition leads to tumor regression or tumor stasis, we evaluated KPC mice for gross tumor diameter by twice-weekly external caliper measurement. Using this approach, we observed that single-agent FAK inhibition increased survival by inducing prolonged tumor stasis rather than regression (**Fig. 2c**). Similar responses were seen in mice bearing orthotopic tumors derived from KI (*Kras*;*INK4A*) or KP (*Kras*;*Trp53*) cells treated with vehicle or FAKi (**Fig. 2d** and **Supplementary Fig. 3b**). Taken together, these data indicate that FAK signaling is an important regulator of PDAC progression, consistent with its observed role in the pathogenesis of other types of cancer[25,26,31].

Inhibition of FAK decreases fibrosis

To determine whether FAK inhibition affects the formation of the otherwise-abundant fibrosis in these tumors, PDAC tissue from end-stage KPC and KPPC mice, as well as KPC mice treated for 1.5 months, was evaluated. We found that FAKi-treated KPC and KPPC mice had markedly reduced levels of fibrosis, as seen by both decreased collagen deposition (Trichrome and Sirius Red staining) and reduced numbers of fibroblasts expressing fibroblast activation protein alpha (FAP) and α-smooth muscle actin (α–SMA) compared with vehicle-treated mice (**Fig. 2e**,**f** and **Supplementary Fig. 3c**–**e**).

To better understand the mechanisms leading to decreased stromal density, we evaluated both tumor and stromal proliferation on the basis of Ki67 staining. We found that even in end-stage KPC and KPPC tumors, PDAC tumor cell proliferation was decreased by 43% in FAKi-treated mice. More notably, PDAC stromal cell proliferation was markedly decreased by up to 87% following FAK inhibition in both KPC and KPPC mice (**Fig. 2g** and **Supplementary Fig. 3f**). This stromal proliferation primarily localized to FAP$^+$ fibroblasts, as observed by IHC (**Fig. 2h**). In addition, expression profiling of PDAC tissue from animals treated with FAKi revealed downregulation of multiple genes associated with fibrosis, collagen deposition and remodeling (**Fig. 2i** and **Supplementary Table 1**). Taken together, these data suggest that FAK inhibition enhances survival by inducing PDAC tumor stasis while simultaneously inducing stromal depletion.

Inhibition of FAK decreases fibrosis without accelerating tumor progression

Recent studies have suggested that depletion of stromal fibrosis has the potential to lead to disease acceleration and more aggressive tumors[9,32]. To assess how stromal depletion by FAKi affects the differentiation and aggressiveness of PDAC tumors, we analyzed pancreatic tumor tissue from end-stage KPC and KPPC animals for tumor stage and grade. We found that, in concert with longer survival, tissue from FAKi- treated KPC mice had a decreased pathologic disease progression when compared with that of vehicle-treated mice (**Fig. 3a** and **Supplementary Fig. 3g**). KPPC mice also showed no evidence of disease acceleration (**Supplementary Fig. 3h**).

As discussed above, FAK signaling has been implicated in tumor invasion, which might explain the suppressed tumor progression observed in KPC mice. To assess this behavior, we used KPC-YFP mice treated at 3.5 months of age with vehicle or FAKi for 1 month and quantified individual invading cells, a hallmark of tumor aggressiveness in this model[33]. We observed significantly reduced numbers of single YFP$^+$ invasive tumor cells (**Fig. 3b**). In correlation with our results from KPC-YFP mice, a short 10-d treatment of mice bearing established orthotopically implanted PDAC tumors with FAKi decreased the frequency of ALDH^{Bright} and CD44^{Hi}CD24^{Hi} tumor cells, indicating a potential reduction in tumor-initiating cells (**Fig. 3c**)[34,35]. Furthermore, we found less liver metastasis in KPC mice treated with FAKi (**Fig. 3d**). Taken together, these data suggest that FAK inhibition diminishes tumor-induced fibrosis, but, unlike recent reports[9,32], reduces disease progression.

Inhibition of FAK decreases immunosuppressive cell populations in tumors

To explore how FAK inhibition might affect immunosuppressive cell populations in PDAC tissue, we analyzed tumor-infiltrating immune cells in KPC mice treated for 1.5 months with vehicle or FAKi. IHC analysis of PDAC tissue showed significantly fewer tumor-infiltrating F4/80$^+$ and CD206$^+$ macrophages and GR1$^+$ granulocytes in FAKi- treated KPC mice (**Fig. 4a**). Consistent with reduced infiltration of suppressive myeloid cell populations, we also observed decreased tumor cell p-STAT3 expression in PDAC tissue (**Fig. 4b**), suggesting a potential signaling mechanism for FAKi effects on

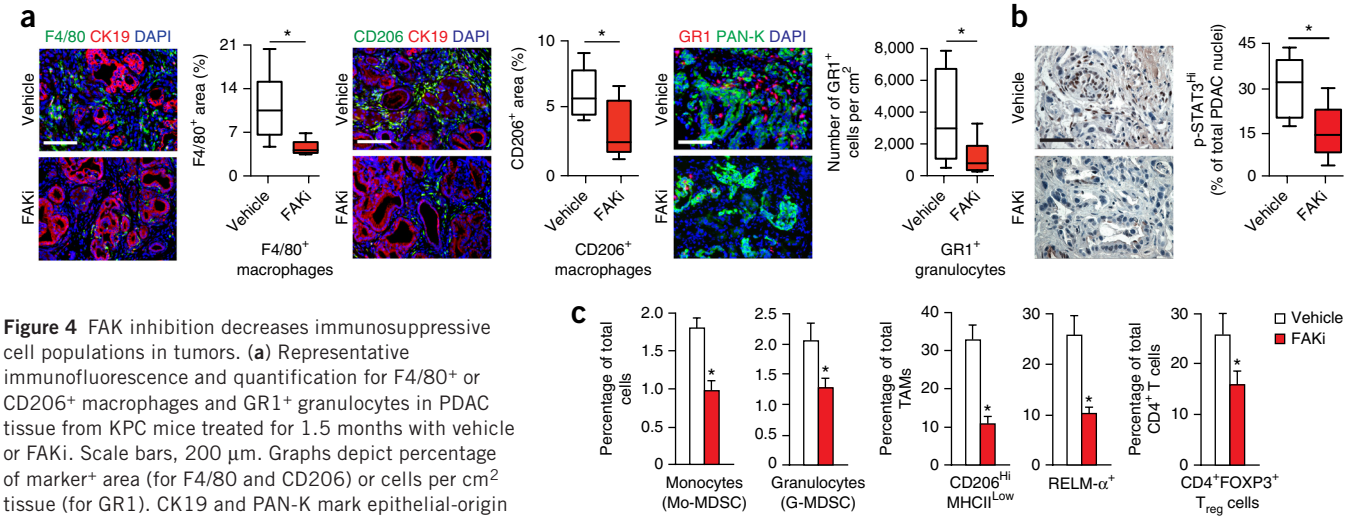

Figure 4 FAK inhibition decreases immunosuppressive cell populations in tumors. (**a**) Representative immunofluorescence and quantification for F4/80$^+$ or CD206$^+$ macrophages and GR1$^+$ granulocytes in PDAC tissue from KPC mice treated for 1.5 months with vehicle or FAKi. Scale bars, 200 µm. Graphs depict percentage of marker$^+$ area (for F4/80 and CD206) or cells per cm^2 tissue (for GR1). CK19 and PAN-K mark epithelial-origin tumor cells. (n = 6–11 mice per group). (**b**) Representative IHC and quantification for p-STAT3 in PDAC tissue from KPC mice treated for 1.5 months with vehicle (top) or FAKi (bottom). Scale bar, 100 µm. Graph depicts percentage of p-STAT3^{High}/PDAC cell nuclei (n = 9 mice per group). (**c**) Flow cytometry analyses of monocytes, granulocytes, TAMs and T_{regs} in PDAC tissue from mice bearing orthotopic KI tumors treated for 10 d with vehicle or FAKi (n = 6 or 7 mice per group). Error bars represent mean ± s.e.m. *P < 0.05 by Student's t-test (**a**–**c**).

immunosuppressive cell infiltration. To confirm these results and to eliminate effects resulting from differing tumor stages, we analyzed mice bearing established orthotopic KI or KP tumors by flow cytometry. We found that, following 10 d of FAKi treatment, the numbers of tumor-infiltrating myeloid-derived suppressor cells (MDSCs), CD206$^+$ tumor-associated macrophages (TAMs) and CD4$^+$FOXP3$^+$ regulatory T cells (T_{regs}) were decreased (**Fig. 4c** and **Supplementary Fig. 4a**,**b**).

To verify that these changes in tumor-infiltrating immunosuppressive cells were not a result of alterations in myelopoiesis, we analyzed bone marrow and blood from mice bearing established KP tumors that were treated for 10 d with FAKi (as described above). During this time period, we observed no change in bone marrow or circulating monocytes, granulocytes, dendritic cells or their precursor populations (**Supplementary Fig. 5a**–**c**). Together, these data suggest that pharmacologic FAK inhibition dampens immunosuppressive inflammatory cell infiltration into PDAC tumors.

Neoplastic cell-intrinsic FAK promotes tumor protective fibrotic and immunosuppressive TME

FAK activity has been implicated in the biologic activity of both neoplastic cells and stromal cells, including endothelial cells, fibroblasts and leukocytes[14,25,36]. These data suggest that FAK is directly involved with both tumor and stromal compartments. The roles of each of these compartments likely contribute to the overall outcome of pharmacologic inhibitors studies. On the basis of our observation that high p-FAK1 levels in the neoplastic cells in human PDACs correlated with fibrosis and inflammatory cell infiltration, we hypothesized that FAK1 activity in tumor cells might be a critical driver of the immunosuppressive PDAC TME. To test this, we knocked down FAK1 in PDAC cells derived from either KPC mice (KP cells) or *p48-Cre/LSL-Kras*^{G12D} mice (KC cells; **Supplementary Fig. 6a**). Perhaps surprisingly, knockdown or pharmacologic inhibition of FAK1 did not suffice to alter cell proliferation *in vitro* under three-dimensional culture conditions (**Fig. 5a**). Notably, concomitant pharmacologic inhibition of both FAK1 and FAK2/PYK2 (FAK1/2i) did indeed succeed in suppressing cell proliferation, suggesting that FAK1 is either dispensable for cell proliferation or compensated for by FAK2/PYK2 expression (**Fig. 5a** and **Supplementary Fig. 6a**,**b**). In contrast with these *in vitro* results, loss of FAK1 alone significantly retarded growth of both KP and KC cells when implanted in syngeneic immune-competent hosts (**Fig. 5b** and **Supplementary Fig. 6c**). Because of these differences in *in vitro* and *in vivo* growth, we postulated that FAK1-deficient cells failed to create a tumor-supportive TME. To test this notion, we analyzed similarly size-matched subcutaneous tumors and short-term orthotopic grafts derived from either shLuc or shFAK1 KP cells. In both settings, we found that reduction of FAK1 expression in the carcinoma cells retarded tumor-induced collagen deposition, FAP$^+$ fibroblast numbers and the presence of Ki67$^+$ fibroblasts (**Fig. 5c** and **Supplementary Fig. 6d**,**e**). In addition, FAK1-deficient tumors had reduced infiltration by MDSCs and CD206$^+$ TAMs (**Fig. 5d**). This reduction in immunosuppressive myeloid cells was accompanied by a marked increase in the numbers of infiltrating CD8$^+$ CTLs (**Fig. 5d**).

These data suggest that FAK1 is required for PDAC cells to create the fibrotic and immunosuppressive TME that protects the tumor from immune surveillance by CTLs. To further explore this notion, we depleted both CD4$^+$ and CD8$^+$ T cells using depleting IgG and found that, although a loss of T cells did not affect outgrowth of control shLuc-expressing KP-derived tumors, it did restore shFAK1-expressing KP tumor growth to control levels (**Fig. 5e**). These findings, in combination with our observations in human tissues, suggest that tumor-intrinsic FAK1 drives the fibrotic and immunosuppressive TME that blunts T cell–mediated immune surveillance.

To understand more precisely how PDAC neoplastic cell-intrinsic FAK1 activity might drive inflammation and fibrosis, we profiled cytokine production from KP cells and found that FAK inhibition markedly reduced both pro-inflammatory and pro-fibrotic cytokine secretion (**Fig. 5f** and **Supplementary Fig. 6f**). We next sought to test whether these alterations in cytokine production would reduce the capacity of PDAC tumor cells to induce myeloid cell recruitment and/or pro-tumor polarization. First, we found that both genetic (shRNA) and pharmacologic inhibition of FAK1 signaling in KP cells

impaired their ability to induce monocyte and granulocyte migration (**Fig. 5g**). Second, we found that, although both murine and human PDAC cell lines were able to induce alternative activation of macrophages, as measured by elevated CD206 or CD163 protein expression and/or elevated *ARG1*, *YM1* and *CCL2* gene expression, this induction was blocked when PDAC cells were pre-treated with FAKi (**Supplementary Fig. 6g–j**). These data suggest that hyper-activated FAK1 in PDAC neoplastic cells drives cytokine production, which in turn results in increased myeloid cell recruitment and pro-tumor polarization of macrophages.

We next sought to more directly assess whether loss of FAK1 might directly affect the ability of PDAC cells to promote expansion of tumor-associated fibroblasts. We noted that the loss of FAK activity in PDAC cells reduced their production of pro-fibrotic factors, such as CCL6, CCL20 and CXCL12 (**Fig. 5f** and **Supplementary Fig. 6f**). We also found that direct co-culture or conditioned medium (CM) from

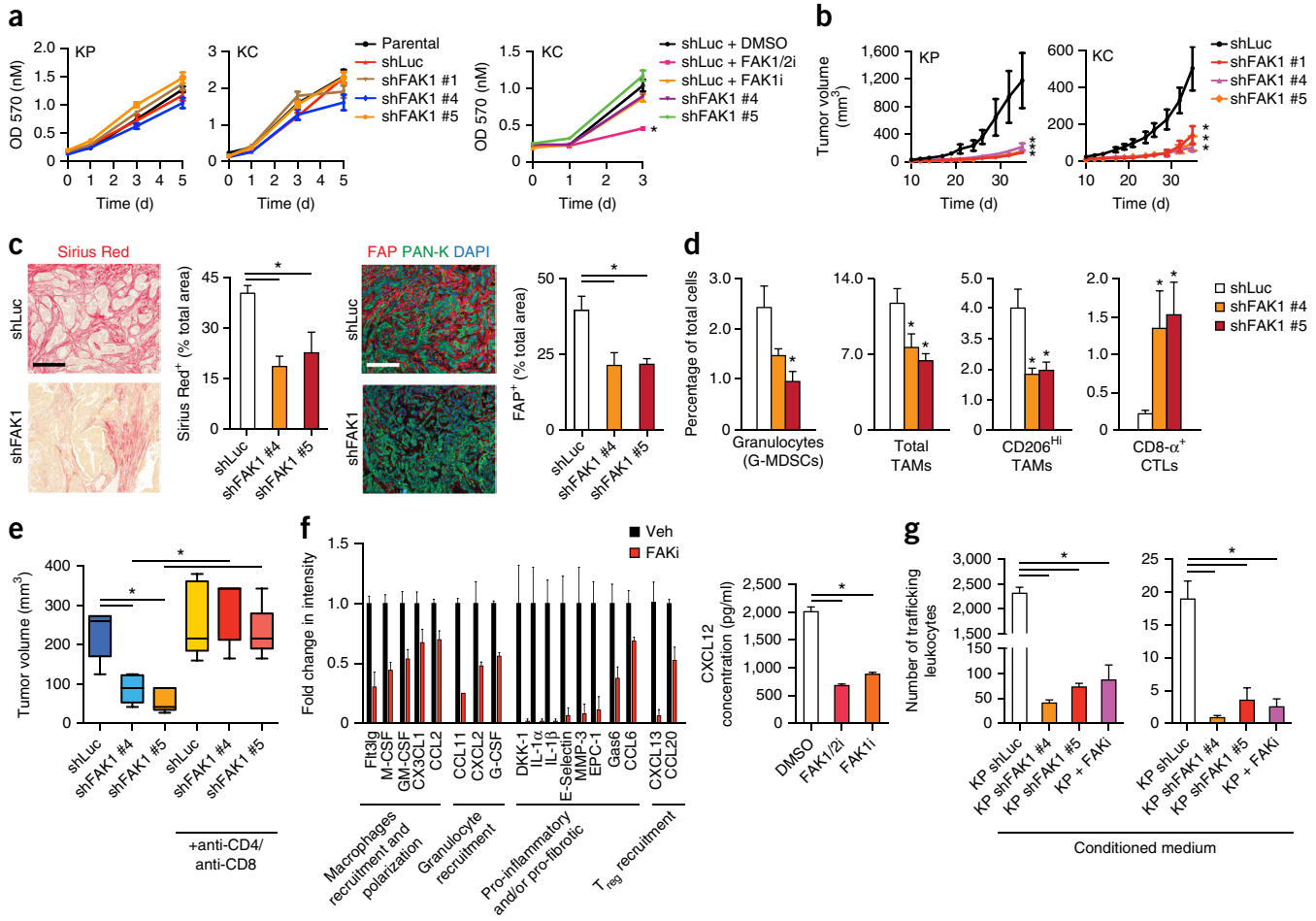

Figure 5 FAK1 in PDAC cells drives fibrosis and immunosuppression. (**a**) *In vitro* growth analysis for KP or KC cells expressing shLuc or shFAK1 constructs, or treated with FAK1/2i (VS-4718) or FAK1i (VS-116). (**b**) Syngeneic tumor growth of KP or KC cells stably expressing shLuc or shFAK1. (**c**) Representative staining and quantification for Sirius Red (left) and FAP (right) in KP tumors expressing shLuc or shFAK1. Scale bars represent 400 µm. (**d**) Flow cytometry analysis of granulocytes, TAMs and CD8$^+$ T cells in KP tumors expressing shLuc or shFAK1. (**e**) *In vivo* subcutaneous tumor burden 25 d after injection with KP cells expressing shLuc or shFAK1. A subset of mice was also treated with CD4- and CD8-depleting IgG starting 1 d before tumor cell injection. (**f**) Cytokine profile of CM from KP cells treated with vehicle or FAKi for 24 h (left) and ELISA for CXCL12 protein expression in CM from KP cells treated with DMSO, FAK1/2i or FAK1i for 24 h (right). (**g**) Flow cytometry analysis of CD11b$^+$Ly6G$^+$ (left) and CD11b$^+$Ly6G$^-$Ly6C$^+$ (right) leukocyte trafficking *in trans*-well system containing different CM. (**h**) Immunofluorescence staining for Ki67 in normal murine pancreas fibroblasts following 24-h treatment with DMSO or FAKi, with CM from parental KP cells ± DMSO or FAKi (left), or CM from KP or KC cells expressing shLuc or shFAK1 (right). (**i**) Immunofluorescence staining for Ki67 in normal murine pancreas fibroblasts following treatment with CM from KP cells cultured on BME ± neutralizing antibodies against CXCL12. All *in vitro* assays are representative of three independent and agreeing replicate experiments. All animal experiments included 5–7 mice per group unless otherwise specified. Error bars represent mean ± s.e.m. $^*P < 0.05$; by one-way ANOVA with Dunnett's multiple-comparison test (**a**–**d**,**f**,**g**) or Student's *t*-test (**e**,**h**,**i**).

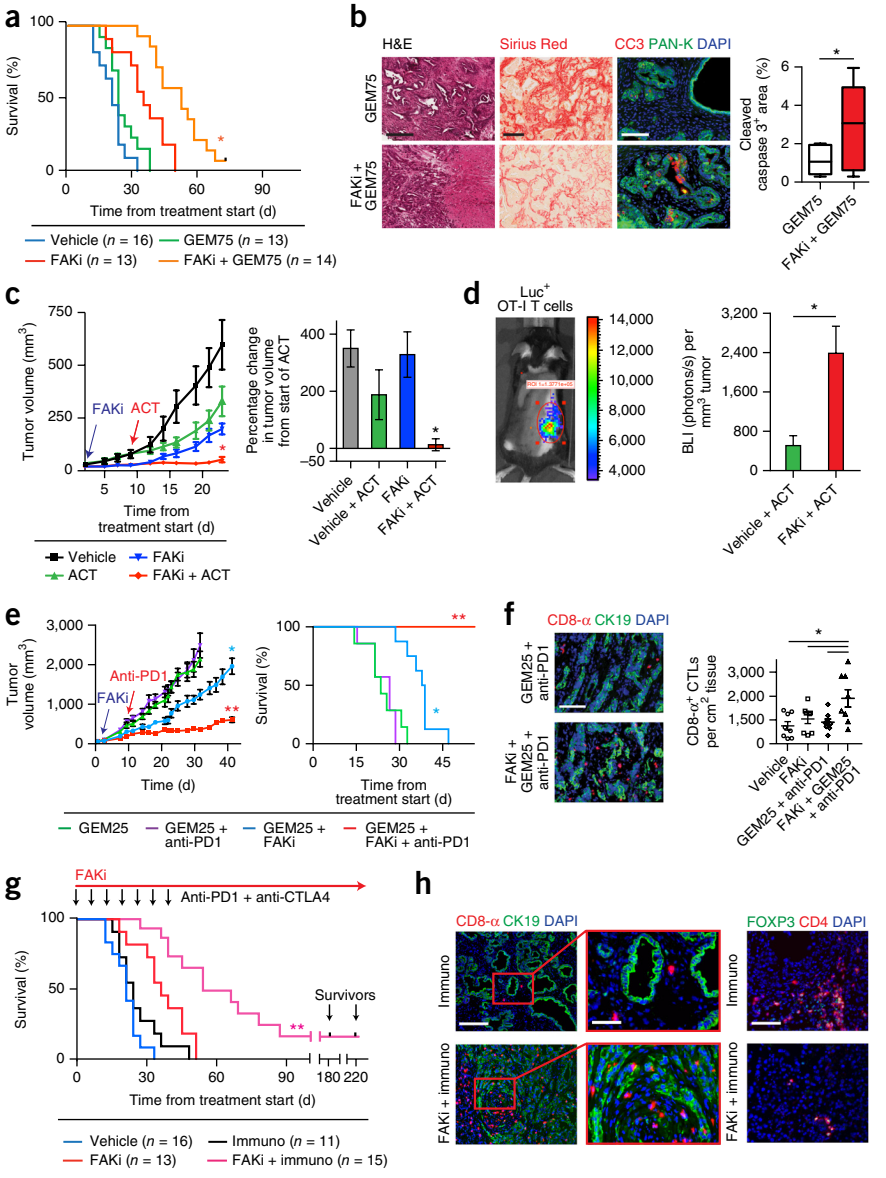

Figure 6 FAK inhibition renders PDAC tumors responsive to chemo- and immunotherapy. (**a**) Kaplan-Meier survival analysis of KPPC mice treated with vehicle or FAKi (VS-4718) ± 75 mg/kg gemcitabine (GEM75). (**b**) Representative H&E (left), Sirius Red (middle) and immunofluorescence (right) staining for cleaved caspase-3 (CC3) and Pan-Keratin (Pan-K) in end-stage tumor tissue from KPPC mice treated with GEM75 (top) or FAKi + GEM75 (bottom). Scale bars, 400 µm (H&E and Sirius Red) and 200 µm (CC3). (**c**) Tumor growth curve of KP–OVA-bearing mice treated with vehicle or FAKi followed by adoptive cell transfer (ACT) of OT-I T cells. Right, percentage change in tumor volume 11 d after ACT. (**d**) *In vivo* bioluminescence imaging (BLI) of luciferase$^+$ OT-I CD8-α$^+$ T cells in KP–OVA-bearing mice 11 d after ACT, with quantification of mean photon flux/tumor volume. (**e**) Tumor growth curve (left) and Kaplan–Meier survival analysis (right) of KP tumor-bearing mice treated as described. (**f**) Representative immunofluorescence staining and quantification for CD8-α$^+$ CTLs and cytokeratin 19 (CK19) in tumor tissues from selected treatment groups. Scale bar, 100 µm. (**g**) Kaplan–Meier survival analysis of KPPC mice treated with vehicle, FAKi, immuno (i.e., GEM25 + anti-PD1/anti-CTLA4), vehicle + immuno, or FAKi + immuno). Black notches indicate animals alive without detectable disease progression after 6 months. (**h**) Representative immunofluorescence staining for CD8-α$^+$ CTLs (left) or CD4$^+$ FOXP3$^+$ T_{regs} (right) in end-stage tumor tissue from KPPC mice. Scale bars, 200 µm for CD8-α and CD4 (magnified field, 100 µm). All values are depicted as mean ± s.e.m. $^*P < 0.05$, $^{**}P < 0.01$; by log-rank test (**a**,**e**,**g**), unpaired two-sided Student's *t*-test (**b**,**d**) or one-way ANOVA with Tukey's method for multiple comparisons (**c**,**e**,**f**). All animal experiments include >7 mice per group unless otherwise specified.

KP or KC cells induced high levels of proliferation in normal pancreatic fibroblasts; however, CM from FAK1-deficient KP or KC cells failed to increase fibroblast proliferation (**Fig. 5h** and **Supplementary Fig. 6k**,**l**). Notably, pharmacologic or genetic inhibition of FAK1 in cancer-associated fibroblasts sorted from KPPC mice did not inhibit cell proliferation *in vitro* (**Supplementary Fig. 6m**,**n**). Neutralization of CXCL12 in CM from KP cells was sufficient to restrict the level of PDAC-induced fibroblast proliferation to basal levels equal to those of fibroblasts treated with CM from FAK1-depleated cells (**Fig. 5i**). These data suggest that FAK1 activity in PDAC cells can drive stromal expansion in part by elevating CXCL12 production.

FAK inhibition renders previously unresponsive PDACs sensitive to chemo- and immunotherapy

Recent studies have shown that stromal depletion may facilitate responses to chemo- and immunotherapy in PDAC[9–11,32]. In addition, excessive tumor infiltration of myeloid cells may further blunt the efficacy of both chemotherapy[4,13,37–41] and immunotherapy[2,42,43]. Given that FAK inhibition reduced both fibrosis and suppressive myeloid cells, we sought to test the ability of FAK inhibition to improve chemo- and immunotherapeutic efficacy.

We first treated KPPC mice bearing overt tumors with either vehicle or high-dose GEM (75 mg per kg of body weight, intravenously (i.v.), GEM75) in the presence or absence of FAKi. Consistent with reported results[10,32,44], we found that GEM75 treatment alone conferred no survival benefits in KPPC mice. In contrast, the combination of FAKi plus GEM75 more than doubled the median survival duration of the mice (**Fig. 6a**). Furthermore, increased PDAC cell apoptosis and tumor necrosis, as well as reduced fibrosis, were observed in end-stage mice (**Fig. 6b** and **Supplementary Fig. 7a**).

To assess the ability of FAK inhibition to improve immunotherapy by increasing T cell infiltration into tumors, we tested FAKi in combination with adoptive T cell transfer (ACT). To evaluate this, we established syngeneic tumors with KP cells expressing chicken ovalbumin (OVA), a potent T cell antigen. We next injected transgenic CD8$^+$ T cells specific for OVA that also expressed CD45.1 and firefly luciferase (CD45.1/CAG-Luc/OT-I) into the tumor bearing mice. Analysis of response to adoptively transferred CD8$^+$ OT-I T cells revealed that,

although ACT alone modestly slowed tumor progression, treatment with FAKi and ACT abrogated tumor growth (**Fig. 6c**). To determine whether the increased efficacy of ACT following FAKi treatment was a result of the increased ability of T cells to infiltrate PDAC tumors, we assessed both circulating and tumor-infiltrating OT-I T cell numbers using flow cytometry and bioluminescent imaging (BLI). We found that, although the number of circulating CD45.1$^+$ OT-I cells was unchanged by FAKi treatment (**Supplementary Fig. 7b**), FAKi treatment still resulted in 4.7-fold more OT-I cells infiltrating into PDAC tumor tissue compared with vehicle-treated mice (**Fig. 6d**). Together, these data suggest that FAKi alters the TME to facilitate CTL infiltration and/or survival in the PDAC TME.

To further test the ability of FAKi to improve immunotherapy, we evaluated several combinations of checkpoint immunotherapies with FAKi in syngeneic and genetic PDAC models. Using both syngeneic and orthotopic models, we found that FAK inhibition promoted the responsiveness to a PD-1 antagonist (anti-PD1), as seen by reduced tumor burden and improved overall survival; however, the maximum effect was seen when given in combination with low-dose GEM (25 mg/kg i.v., GEM25; **Fig. 6e** and **Supplementary Fig. 7c**). We also found that mice bearing transplantable KP tumors that were treated with FAKi + GEM25 + anti-PD1 had a significantly increased number of tumor-infiltrating CD8$^+$ CTLs compared with vehicle + GEM25 + anti-PD1 treated mice (**Fig. 6f**). Notably, FAKi did not improve the responsiveness to anti-CTLA4 alone, but anti-CTLA4 did show added benefit when added to FAKi + GEM25 + anti-PD1 therapies (**Supplementary Fig. 7d,e**).

We next sought to test FAKi plus immunotherapy in the KPPC transgenic mice, as this mouse model recapitulates the poor immunogenicity and rapid progression typical of human pancreatic cancer. Treatment of KPPC mice with GEM25 + anti-PD1 + anti-CTLA4 (Immuno) did not alter survival compared to vehicle-treated mice, suggesting that KPPC mice had little *de novo* responsiveness to checkpoint immunotherapy. By contrast, KPPC mice treated with FAKi + GEM25 + anti-PD1/anti-CTLA4 showed a greater than 2.5-fold increase in median survival time, with a subset of mice (2 of 15) still alive 6 months after the start of treatment (**Fig. 6g**). This observed improvement in immunotherapeutic efficacy was associated with increased numbers of CD8$^+$ CTLs that penetrated the stroma and came into close proximity and/or contact with target CK19$^+$ PDAC cells; at the same time, these tumors exhibited reduced numbers of CD4$^+$ FOXP3$^+$ T_{regs}, and better T effector (T_{eff}) to T_{reg} ratios in the tumors (**Fig. 6h** and **Supplementary Fig. 7f**). Taken together, these data indicate that FAK inhibition, which diminished the fibrotic and immunosuppressive TME, can render previously unresponsive PDAC tumors responsive to chemo- and immunotherapy.

DISCUSSION

We found that FAK signaling is a key driver of fibrosis, immunosuppression and PDAC progression. Several FAK inhibitors are in clinical testing now; to date, however, FAK inhibitors as single agents have failed to induce tumor regression in advanced cancer patients. Our own data in murine PDAC models agree with this, as we observed disease stabilization rather than PDAC regression in KPC mice (**Fig. 2c**). These data are consistent with results from the completed phase I study of single agent FAK inhibition (VS-6063/PF-00562271) in patients with advanced solid tumors, NCT00787033. In this study, 43% (16 of 37) of patients enrolled at doses >100 mg experienced stable disease. One of these patients had PDAC and had stable disease on single-agent FAK inhibition for >6 months. These clinical data suggest that FAKi combination therapies may be important for achieving durable tumor regression in advanced cancer patients. In our hands, pharmacologic or genetic targeting of FAK augmented tumor immunity, and thereby potentiated the efficacy of chemo- and immunotherapy, even in PDAC tumors that were previously unresponsive to these therapies. Our data strongly support the translation of FAK inhibitors in combination with checkpoint immunotherapy, an approach that is currently undergoing clinical trials (NCT02546531).

Given that many FAK inhibitors, including the one we employed, are active against both FAK1 and FAK2/PYK2, it is important to consider the roles of each of these kinases. We found that FAK1 in PDAC cells can be a driver of tumor-induced fibrosis and immune suppression (**Fig. 5**). However, this does not exclude a potentially critical role of FAK2/PYK2 in regulating fibrosis and/or immune suppression in response to dual FAK1-PYK2 inhibitors, such as VS-4718 or others undergoing clinical trials. We found that both FAK2/PYK2 and phospho-PYK2 were elevated in human and murine PDACs (**Supplementary Fig. 1f,g**). In addition, PYK2 has been shown to be important in wound healing, fibrosis, and myeloid cell migration and differentiation[19–24]. Thus, a further dissection of the exact contribution of both FAK1 and PYK2 in driving fibrotic and immunosuppressive TMEs will be critical to exploiting FAK inhibition to benefit cancer patients.

We focused on the role of FAK1 signaling in malignant cells and its role as a driver of the fibrotic and inflammatory TME that thwarts immune surveillance and limits immunotherapy. However, clinical use of FAK inhibitors will target all cell types, including T cells themselves[45–48]. Both FAK1 and PYK2 are activated downstream of both T cell receptor and co-stimulatory signaling, and have been shown to be involved in T cell proliferation, antigen sensitivity, cytokine production and migration in these contexts (reviewed in ref. 47). We found no alterations in total circulating T cells or transferred antigen-specific T cell numbers following pharmacologic inhibition of FAK1 and PYK2; however, the effect of such treatments on T cell functionality is likely important to clinical translation of FAK inhibitor and immunotherapeutic combinations.

FAK signaling has been confirmed as a regulator of multiple signaling pathways during tumor progression, including cell-cell adhesion, migration, proliferation and chemokine transcription[14]. As such, FAK1 has been shown to be important in several carcinoma types, including pancreatic tumors[14,26,49–53]. However, the role of FAK signaling in driving the suppressive tumor microenvironment is less well understood. A recent study in squamous carcinoma mouse models found that nuclear FAK1 in carcinoma cells drives exhaustion of CD8$^+$ T cells and recruitment of T_{regs} to the TME by altering chemokine/cytokine networks[15]. Similarly, we found that FAK inhibition altered tumor cell production of pro-inflammatory and immunosuppressive cytokines and blunted their ability to avoid immune surveillance. Together, these findings indicate that FAK1 signaling may be a key driver of immune escape in several tumor types, and thus may be a target for combination with immunotherapy.

METHODS

Methods and any associated references are available in the online version of the paper.

Accession codes. GSE75233.

ACKNOWLEDGMENTS

KC (*Kras*^{G12D}) cells were obtained from P. Mukherjee (University of North Carolina). HPNE, HPAC, Capan-1, Capan-2, Hs766T, MIA PaCa-2 and SW1990 cells were obtained from K. Lim (Washington University). pBABEpuro K-Ras G12V

used to express $Kras^{G12V}$ was obtained from J. Weber (Washington University). This work was supported by funding awarded to D.G.D. by Lustgarten Foundation, an AACR/PANCAN Award, NCI awards R01-CA177670, R01-CA203890 and R21-CA182701, the BJCIH/Siteman Cancer Center Cancer Frontier Fund, and Washington University Clinical and Translational Grant KL2TR000450 awarded to A.W.G.

AUTHOR CONTRIBUTIONS

D.G.D. managed the project and coordinated activities from all authors. H.J. conducted transgenic and transplant mouse experiments and treatments. B.L.K. and J.M.H. aided with FAK inhibitor treatments. D.G.D., H.J. and B.L.K. designed experiments and provided KPC, KPPC and KPC-Y mice. D.G.D., S.H. and J.M.H. performed histology, immunofluorescence on human samples and related analyses. H.J. and S.H. conducted experiments with the PA hydrogels. H.J. performed MTT (3-(4,5-dimethylthiazolyl-2)-2,5-diphenyltetrazolium bromide), three-dimensional collagen assays, cytokine arrays, leukocyte trafficking, immunoblotting and related analyses. S.H. and J.M.H. performed immunofluorescence and H.J. conducted analysis. H.J. and B.L.K. conducted subcutaneous and orthotropic PDAC mouse experiments. S.H. and H.J. conducted adoptive cell transfer and bioluminescence tracking. Y.Z. performed reverse transcription PCR and flow analysis in bone marrow macrophage experiments. M.A.M. performed bone marrow flow analysis. D.G.D. and H.J. conducted PDAC tumor grading in transgenic mice. T.M.N., W.G.H. and A.W.-G. collected human samples and aided with pathological pancreatic cancer scoring of human samples. I.M.S., D.T.W. and J.A.P. provided FAK inhibitor VS-4718 and VS-116, as well as expert guidance and intellectual input on the project. D.G.D., H.J. and S.H. wrote the manuscript with input from all authors.

COMPETING FINANCIAL INTERESTS

The authors declare competing financial interests: details are available in the online version of the paper.

1. Royal, R.E. *et al.* Phase 2 trial of single agent Ipilimumab (anti-CTLA-4) for locally advanced or metastatic pancreatic adenocarcinoma. *J. Immunother.* **33**, 828–833 (2010).
2. Zhu, Y. *et al.* CSF1/CSF1R blockade reprograms tumor-infiltrating macrophages and improves response to T cell checkpoint immunotherapy in pancreatic cancer models. *Cancer Res.* **74**, 5057–5069 (2014).
3. Panni, R.Z., Linehan, D.C. & DeNardo, D.G. Targeting tumor-infiltrating macrophages to combat cancer. *Immunotherapy* **5**, 1075–1087 (2013).
4. Mitchem, J.B. *et al.* Targeting tumor-infiltrating macrophages decreases tumor-initiating cells, relieves immunosuppression and improves chemotherapeutic responses. *Cancer Res.* **73**, 1128–1141 (2013).
5. Goedegebuure, P. *et al.* Myeloid-derived suppressor cells: general characteristics and relevance to clinical management of pancreatic cancer. *Curr. Cancer Drug Targets* **11**, 734–751 (2011).
6. Bayne, L.J. *et al.* Tumor-derived granulocyte–macrophage colony-stimulating factor regulates myeloid inflammation and T cell immunity in pancreatic cancer. *Cancer Cell* **21**, 822–835 (2012).
7. Laklai, H. *et al.* Genotype tunes pancreatic ductal adenocarcinoma tissue tension to induce matricellular fibrosis and tumor progression. *Nat. Med.* **22**, 497–505 (2016).
8. Feig, C. *et al.* Targeting CXCL12 from FAP-expressing carcinoma-associated fibroblasts synergizes with anti-PD-L1 immunotherapy in pancreatic cancer. *Proc. Natl. Acad. Sci. USA* **110**, 20212–20217 (2013).
9. Özdemir, B.C. *et al.* Depletion of carcinoma-associated fibroblasts and fibrosis induces immunosuppression and accelerates pancreas cancer with reduced survival. *Cancer Cell* **25**, 719–734 (2014).
10. Olive, K.P. *et al.* Inhibition of Hedgehog signaling enhances delivery of chemotherapy in a mouse model of pancreatic cancer. *Science* **324**, 1457–1461 (2009).
11. Provenzano, P.P. *et al.* Enzymatic targeting of the stroma ablates physical barriers to treatment of pancreatic ductal adenocarcinoma. *Cancer Cell* **21**, 418–429 (2012).
12. Beatty, G.L. *et al.* Exclusion of T cells from pancreatic carcinomas in mice is regulated by Ly6ClowF4/80+ extratumoral macrophages. *Gastroenterology* **149**, 201–210 (2015).
13. Sanford, D.E. *et al.* Inflammatory monocyte mobilization decreases patient survival in pancreatic cancer: a role for targeting the CCL2–CCR2 axis. *Clin. Cancer Res.* **19**, 3404–3415 (2013).
14. Sulzmaier, F.J., Jean, C. & Schlaepfer, D.D. FAK in cancer: mechanistic findings and clinical applications. *Nat. Rev. Cancer* **14**, 598–610 (2014).
15. Serrels, A. *et al.* Nuclear FAK controls chemokine transcription, T_{regs} and evasion of antitumor immunity. *Cell* **163**, 160–173 (2015).
16. Tavora, B. *et al.* Endothelial cell FAK targeting sensitizes tumors to DNA-damaging therapy. *Nature* **514**, 112–116 (2014).
17. Zhao, X.K. *et al.* Focal adhesion kinase regulates fibroblast migration via integrin β-1 and plays a central role in fibrosis. *Sci. Rep.* **6**, 19276 (2016).
18. Balasubramanian, S. *et al.* Dasatinib attenuates pressure overload induced cardiac fibrosis in a murine transverse aortic constriction model. *PLoS One* **10**, e0140273 (2015).
19. Rustad, K.C., Wong, V.W. & Gurtner, G.C. The role of focal adhesion complexes in fibroblast mechanotransduction during scar formation. *Differentiation* **86**, 87–91 (2013).
20. Sonomura, K. *et al.* The kinase Pyk2 is involved in renal fibrosis by means of mechanical stretch-induced growth factor expression in renal tubules. *Kidney Int.* **81**, 449–457 (2012).
21. You, K., Huang, Y., Zhang, M.C. & Hao, J. Control and prevention of myocardial fibrosis using Pyk2-related non-kinase. *Int. J. Clin. Exp. Med.* **8**, 18284–18292 (2015).
22. Koppel, A.C. *et al.* Delayed skin wound repair in proline-rich protein tyrosine kinase 2–knockout mice. *Am. J. Physiol. Cell Physiol.* **306**, C899–C909 (2014).
23. Graves, D.T., Wu, Y. & Badadani, M. Pyk2 contributes to re-epithelialization by promoting MMP expression. Focus on 'Delayed skin wound repair in proline-rich protein tyrosine kinase 2–knockout mice'. *Am. J. Physiol. Cell Physiol.* **306**, C887–C888 (2014).
24. Okigaki, M. *et al.* Pyk2 regulates multiple signaling events crucial for macrophage morphology and migration. *Proc. Natl. Acad. Sci. USA* **100**, 10740–10745 (2003).
25. Stokes, J.B. *et al.* Inhibition of focal adhesion kinase by PF-562,271 inhibits the growth and metastasis of pancreatic cancer concomitant with altering the tumor microenvironment. *Mol. Cancer Ther.* **10**, 2135–2145 (2011).
26. Konstantinidou, G. *et al.* RHOA–FAK is a required signaling axis for the maintenance of KRAS-driven lung adenocarcinomas. *Cancer Discov.* **3**, 444–457 (2013).
27. Bae, Y.H. *et al.* A FAK–Cas–Rac–lamellipodin signaling module transduces extracellular matrix stiffness into mechanosensitive cell cycling. *Sci. Signal.* **7**, ra57 (2014).
28. Kümper, S. & Marshall, C.J. ROCK-driven actomyosin contractility induces tissue stiffness and tumor growth. *Cancer Cell* **19**, 695–697 (2011).
29. Samuel, M.S. *et al.* Actomyosin-mediated cellular tension drives increased tissue stiffness and β-catenin activation to induce epidermal hyperplasia and tumor growth. *Cancer Cell* **19**, 776–791 (2011).
30. Wozniak, M.A., Desai, R., Solski, P.A., Der, C.J. & Keely, P.J. ROCK-generated contractility regulates breast epithelial cell differentiation in response to the physical properties of a three-dimensional collagen matrix. *J. Cell Biol.* **163**, 583–595 (2003).
31. Pylayeva, Y. *et al.* Ras- and PI3K-dependent breast tumorigenesis in mice and humans requires focal adhesion kinase signaling. *J. Clin. Invest.* **119**, 252–266 (2009).
32. Rhim, A.D. *et al.* Stromal elements act to restrain, rather than support, pancreatic ductal adenocarcinoma. *Cancer Cell* **25**, 735–747 (2014).
33. Rhim, A.D. *et al.* EMT and dissemination precede pancreatic tumor formation. *Cell* **148**, 349–361 (2012).
34. Kim, M.P. *et al.* ALDH activity selectively defines an enhanced tumor-initiating cell population relative to CD133 expression in human pancreatic adenocarcinoma. *PLoS One* **6**, e20636 (2011).
35. Hermann, P.C. *et al.* Distinct populations of cancer stem cells determine tumor growth and metastatic activity in human pancreatic cancer. *Cell Stem Cell* **1**, 313–323 (2007).
36. Crompton, B.D. *et al.* High-throughput tyrosine kinase activity profiling identifies FAK as a candidate therapeutic target in Ewing sarcoma. *Cancer Res.* **73**, 2873–2883 (2013).
37. DeNardo, D.G. *et al.* Leukocyte complexity predicts breast cancer survival and functionally regulates response to chemotherapy. *Cancer Discov.* **1**, 54–67 (2011).
38. Ruffell, B. *et al.* Macrophage IL-10 blocks CD8+ T cell–dependent responses to chemotherapy by suppressing IL-12 expression in intratumoral dendritic cells. *Cancer Cell* **26**, 623–637 (2014).
39. Strachan, D.C. *et al.* CSF1R inhibition delays cervical and mammary tumor growth in murine models by attenuating the turnover of tumor-associated macrophages and enhancing infiltration by CD8+ T cells. *OncoImmunology* **2**, e26968 (2013).
40. Shree, T. *et al.* Macrophages and cathepsin proteases blunt chemotherapeutic response in breast cancer. *Genes Dev.* **25**, 2465–2479 (2011).
41. Beatty, G.L. *et al.* Mesothelin-specific chimeric antigen receptor mRNA–engineered T cells induce antitumor activity in solid malignancies. *Cancer Immunol. Res.* **2**, 112–120 (2014).
42. Highfill, S.L. *et al.* Disruption of CXCR2-mediated MDSC tumor trafficking enhances anti-PD1 efficacy. *Sci. Transl. Med.* **6**, 237ra67 (2014).
43. Mok, S. *et al.* Inhibition of CSF-1 receptor improves the antitumor efficacy of adoptive cell transfer immunotherapy. *Cancer Res.* **74**, 153–161 (2014).
44. Beatty, G.L. *et al.* CD40 agonists alter tumor stroma and show efficacy against pancreatic carcinoma in mice and humans. *Science* **331**, 1612–1616 (2011).

45. Chapman, N.M. & Houtman, J.C. Functions of the FAK family kinases in T cells: beyond actin cytoskeletal rearrangement. *Immunol. Res.* **59**, 23–34 (2014).
46. Chapman, N.M., Connolly, S.F., Reinl, E.L. & Houtman, J.C. Focal adhesion kinase negatively regulates Lck function downstream of the T cell antigen receptor. *J. Immunol.* **191**, 6208–6221 (2013).
47. Chapman, N.M., Yoder, A.N. & Houtman, J.C. Noncatalytic functions of Pyk2 and Fyn regulate late stage adhesion in human T cells. *PLoS One* **7**, e53011 (2012).
48. Collins, M., Bartelt, R.R. & Houtman, J.C. T cell receptor activation leads to two distinct phases of Pyk2 activation and actin cytoskeletal rearrangement in human T cells. *Mol. Immunol.* **47**, 1665–1674 (2010).
49. Stewart, J.E. *et al.* Inhibition of FAK and VEGFR-3 binding decreases tumorigenicity in neuroblastoma. *Mol. Carcinog.* **54**, 9–23 (2015).
50. Golubovskaya, V. *et al.* Downregulation of ALDH1A3, CD44 or MDR1 sensitizes resistant cancer cells to FAK autophosphorylation inhibitor Y15. *J. Cancer Res. Clin. Oncol.* **141**, 1613–1631 (2015).
51. Zheng, D. *et al.* A novel strategy to inhibit FAK and IGF-1R decreases growth of pancreatic cancer xenografts. *Mol. Carcinog.* **49**, 200–209 (2010).
52. Hochwald, S.N. *et al.* A novel small-molecule inhibitor of FAK decreases growth of human pancreatic cancer. *Cell Cycle* **8**, 2435–2443 (2009).
53. François, R.A. *et al.* Targeting focal adhesion kinase and resistance to mTOR inhibition in pancreatic neuroendocrine tumors. *J. Natl. Cancer Inst.* **107**, djv123 (2015).

ONLINE METHODS

Pancreatic cancer tissue analysis. Tissue microarray (TMA) studies were conducted on surgically resected PDAC specimens from 56 patients diagnosed in the Department of Pathology at Washington University. Patients underwent pancreaticoduodenectomy followed by adjuvant chemotherapy (no neoadjuvant therapy). Clearly defined tumor areas were demarcated and two biopsies (1.0-mm diameter) were taken from each donor block for 4.0-μm paraffin sections. The Washington University School of Medicine Ethics committee approved this study under protocol 2011103202. All tissue samples were collected for analysis under informed consent from the patients. Automated image acquisition was performed using an Aperio ScanScope XT Slide Scanner system with a 20× objective (Aperio Technologies). In individual analyses, patients lacking survival data or whose tissue cores were unreadable/exhausted were excluded.

Genetic mouse models. KPC (*p48-Cre*;*LSL-Kras*^{G12D};*Trp53*$^{flox/+}$), KPPC (*p48-Cre*;*LSL-Kras*^{G12D};*Trp53*$^{flox/flox}$), KPC-Y (*p48-Cre*;*LSL-Kras*^{G12D};*Trp53*$^{flox/+}$;*LSL-YFP*) were created by breeding C57/B6 *LSL-Kras*^{G12D};*Trp53*^{Flox} or *LSL-YFP* mice (Jax mice) to *p48-Cre* mice that had been backcrossed $n = 6$ times to C57BL/6. Congenic marker analysis was used to verify the C57BL/6 identity of KPC and KPPC colony founder mice. For all experiments, KPC/KPPC mice were either enrolled when age-matched and/or after first >0.5 cm tumor was detected by weekly palpation. Survival events were scored when mice lost >15% body weight, tumor burden reached > 1.8 cm in diameter or per absolute survival events. Transgenic OT-I mice and CAG-Luc-eGFP mice were obtained from Jackson laboratory and bred together to create CAG-Luc$^+$/OT-I$^+$ mice. Non-transgenic C57BL/6 or FVB/N mice were obtained from either Jackson Laboratory or Charles River. Mice were maintained within the Washington University Laboratory for Animal Care barrier facility. The Washington University School of Medicine Institutional Animal Studies Committee approved all studies involving animals.

Cell lines, plasmids, shRNAs and siRNAs. KP cells were derived from PDAC tumor tissue obtained from 6-month-old *p48-Cre*;*LSL-Kras*^{G12D};*Trp53*$^{flox/+}$ mice, which were screened for C57BL/6 identity. Cells were grown out on collagen-coated plastic for <12 passages and were tested for CK19, SMA, Vimentin and CD45 to verify their identity and purity. Primary pancreatic fibroblasts were isolated from normal pancreas of 8-week-old female mice. Cancer-associated fibroblasts (CAFs) were flow-sorted from KPC tumor tissue using marker CD45$^-$Pan-keratin$^-$ PDGFR-α$^+$ (clone APA5, eBioscience) and used within 4–6 passages for all experiments. All cell lines were tested negative for MAP and mycoplasma.

Short hairpin RNA (shRNA) constructs targeting mouse *Fak1* (*Ptk2*) and *Kras* were purchased from Genome Center (Washington University). Targeting sequences are listed in **Supplementary Table 2**.

To generate cell lines stably expressing shFAK1/shKras, KP cells were transduced with lentivirus particles carrying shRNA for 48 h, following standard transduction protocols. Subsequently, cells were cultured in regular DMEM+F12 medium (Gibco) containing 7 μg/mL puromycin (Sigma-Aldrich) for 2 weeks. Surviving cells were tested for knockdown efficiency by western blot. To generate KP-OVA cell line, KP cells were transduced with pLVX-IRES-Hyg-OVA (Clontech) following standard lentiviral protocol. Transduced cells were kept under 200 μg/mL Hygromycin selection during passages. Full-length OVA expression was verified by western blot.

Small interfering RNAs (siRNAs) targeting mouse FAK1 were purchased from Integrated DNA Technologies (IDT). Sequences are listed in **Supplementary Table 2**.

Orthotopic and transplantable models; preclinical animal cohorts. Age-matched 6–8-week-old female C57BL/6 and FVB/N mice were used for orthotopic/transplantable mouse models. Syngeneic orthotopic PDAC tumors were established by surgical implantation, as previously described[54]. Briefly, 200,000 cells in 50 μL Cultrex BME (Trevigen) were injected into each pancreas. Cohorts of mice were randomized into different treatment groups by gross tumor diameter using twice-weekly palpation and external caliper measurement. In establishing transplantable models, 200,000 cells in 50 μL Cultrex BME were injected into each mouse's back. Cohorts of mice were randomized into different treatment groups by tumor volume (length × (width2)/2).

Gemcitabine (GEM; Hospira) was obtained from the Washington University School of Medicine pharmacy and diluted in phosphate-buffered saline (PBS). Mice were treated with GEM by i.v. injection into the right retro-orbital sinus every 4–5 days. Preclinical studies were conducted with 10–15 10-week-old female mice per group. Tumor burden was measured by establishing gross wet weight of the pancreas and comparing it to that of five parallel mice sacrificed at the beginning of treatment.

Inhibitors, neutralizing antibodies and checkpoint antagonists. FAKis were provided by Verastem, Inc. VS-4718 is a selective bispecific inhibitor with activity against FAK1/FAK and FAK2/PYK2 kinases. Cell-based assays have determined it has biochemical half-maximal inhibitory concentrations (IC_{50}) of 6.0 nM and 20 nM for FAK1 and PYK2. For animal experiments, 50 mg/kg VS-4718 was formulated in vehicle (0.5% carboxymethyl cellulose and 0.1% Tween-80 (Sigma-Aldrich) in sterile water) and administered by oral gavage twice a day. For *in vitro* studies 0.5 or 1.0 μM of VS-4718 in DMSO was used. VS-116 is a FAK1-selective inhibitor provided by Verastem, Inc. with IC_{50} of 78 nM and >10 μM for FAK1 and PYK2 respectively, and was employed at 1.0 μM for *in vitro* studies. VS-116 was deemed to be poorly potent for use *in vivo*. For immunotherapy regimen, CTLA4 and PD1 antagonists (anti-mCTLA4 clone UC10-4F10-11; anti-mPD1 clone RMP1-14, BioXCell) were given by intraperitoneal (i.p.) injection every 4–5 d at 250 and 200 μg, respectively. For T cell depletion, CD4- and CD8- neutralizing IgG antibodies (anti-mCD4 clone GK1.5, anti-mCD8 clone 2.43, BioXCell) were administered via i.p. injection every 4–5 d, with the first injection containing 500 μg before tumor implantation and subsequent injections containing 250 μg. For CXCL12 neutralization, normal pancreatic fibroblasts were treated with conditioned medium (CM) from KP tumor cells and either 200 ng, 400 ng, 1.0 μg or 2.0 μg CXCL12 neutralizing antibody (Monoclonal IgG1 Clone 79014, R&D) or mouse IgG control. For ROCK inhibition, KP cells were treated with 10 μM Y-27632 (Tocris Bioscience) for 24 h before fixation and p-FAK immunostaining.

Flow cytometry analysis and flow sorting. Flow cytometry was carried out as described previously[2]. ALDEFLUOR analysis was done according to manufacturer's recommendations (StemCell Tech.). Data acquisition was performed on the LSR-II system (BD Biosciences), and FlowJo v10.0.7r2 (Tree Star) was used for analysis with appropriate compensation. Flow sorting was performed using the FACS Aria-II cell sorter (BD Biosciences). For all sorting experiments, post-sort analyses were performed to ensure >90% purity. All antibodies used for flow cytometry are listed in **Supplementary Table 3**.

Isolation and analyses of human CD14$^+$ monocytes. Leukoreduction chambers from normal donor were obtained from the BJH Pheresis Center (Washington University). Human peripheral blood mononuclear cells (PBMCs) were isolated using a lab protocol provided by T. Fehniger (Washington University). Briefly, chamber eluate was mixed well with PBS containing 1 unit/mL heparin, centrifuged with brakes-off and 'buffy layer' was isolated. Tube was centrifuged at 1,800 rpm for 10 min and pellets were incubated in 1X RBC lysis buffer. After subsequent centrifugation at 1,300 rpm for 4 min, PBMC pellets were resuspended in RPMI containing 10% human AB serum (Sigma-Aldrich). Human CD14$^+$ monocytes were sorted from PBMCs using EasySep Human CD14 Selection Kit (Stemcell Technologies) per manufacturer's instructions. CD14$^+$ monocyte isolation purity >90% was confirmed by flow cytometry. Flow cytometry was conducted as described elsewhere.

Isolation of murine bone marrow–derived macrophages (BM-MACs). Bone marrow-derived macrophages were isolated following the protocol described previously[55]. Briefly, bone marrow cells were isolated by flushing femurs and tibias from C57BL/6 mice and cultured in RPMI-1640 medium (Gibco) containing 10% FBS and 20 ng/mL macrophage colony–stimulating factor (M-CSF, PeproTech) on plastic petriplates. After 7 d in culture, adherent macrophages were harvested for co-culture experiments.

Adoptive cell transfer of Luc$^+$ OT-I T cells. Total splenocytes were harvested from 10-week-old CAG-Luc/OT-I mice and plated in T cell medium, that is,

45% DMEM, 45% RPMI (Gibco), 10% FBS (Atlanta biologicals), 1× β-mercaptoethanol and 1× Pen-Strep (Gibco) with 0.5 μg/mL SIINFEKL peptide (Sigma-Aldrich) and 10 ng/mL IL-2 (PeproTech) for 3 d. Fresh T cell medium was replenished with 0.5 μg/mL SIINFEKL peptide and 10 ng/mL IL-2 on day 2. Cultured splenocytes were collected on Day 3, spun down and enriched for CD8-α^+ T cells using CD8-α microbeads and MACS LS columns (Miltenyi biotec) per manufacturer's instructions. CD8-α^+ T cell isolation purity >90% was confirmed by flow cytometry. Isolated CD8-α^+ T cells were counted and resuspended to desired concentration (15 million cells/mL) in 1× ice-cold DPBS. 50 μL T cell suspension was injected into the right retro-orbital sinus of either FAKi- or vehicle-treated C57BL/6 mice bearing palpable (~0.5 cm) subcutaneous KP-OVA tumors on day 0 and day 1 of ACT regimen.

Bioluminescence imaging. FAKi- or vehicle-treated C57BL/6 mice bearing subcutaneous KP-OVA tumors and having undergone ACT were shaved and epilated before imaging on the Xenogen IVIS-50 Bioluminescence Imaging System (PerkinElmer). Mice were injected with D-luciferin i.p. and tumors imaged at the peak of luciferase activity (10 min post injection, 5-min exposure). Total flux read was analyzed restricted to tumor ROI on Living Image v2.60.1 (Imaging systems) and normalized to unresected tumor volume.

Preparation of polyacrylamide and collagen type I gels. Polyacrylamide gels of ~70-μm nominal thickness and differing stiffness were synthesized on 20-mm glass-bottom dishes (MatTek) as described previously[56]. PAA gels were functionalized by Sulfo-SANPAH crosslinking (Pierce) and subsequent incubation overnight in different ECM protein concentrations as per manufacturer's instructions. ECM proteins used included laminin (Sigma-Aldrich) and fibronectin (Corning). ECM-coated gel dishes were used for culturing KP cells over 24 h before fixation and p-FAK immunostaining. Collagen type I gels were prepared according to manufacturers' instructions. The polymer was placed in an 8-well chamber slide (Lab-Tek II; Thermo Fisher Scientific) and incubated in a 37 °C incubator for 30 min. KP cells were grown on top of gel in complete medium containing 5% FBS for 24 h before fixation and p-FAK immunostaining.

Cell proliferation assay. Cell proliferation assay was performed by using CellTiter96 Non-Radioactive Cell Proliferation Assay (Promega) according to manufacturers' instructions. Briefly, 5,000 cells/well were seeded into 96-well plates coated with 7.5 mg/mL Cultrex BME (Trevigen). At desired time points, Dye Solution was added to live cultures for 4 h at 37 °C. Absorbance was measured at 570 nm on Multiskan GO plate reader (Thermo Fisher Scientific).

Leukocyte tracking assay. Peripheral blood was collected from left ventricles of anesthetized 8-week old healthy C57BL/6 mice into 1× PBS containing heparin (1 unit/mL) on ice. Blood was centrifuged at 2,000 rpm for 5 min, and RBCs were lysed using 1× RBC Lysis Buffer (BioLegend). Subsequently, cells were centrifuged, resuspended in serum-free DMEM+F12 medium and counted by Trypan Blue staining. For trans-well assays, 1 mL of tumor CM containing 5% FBS was added to bottom of 24-well plate. 5×10^5 leukocytes were added to upper chamber of 24-well trans-well inserts (3 μm, Corning). Cells were incubated at 37 °C for 6 h, following which inserts were removed, cells in lower well were resuspended in 1 mL DMEM and counted using hemocytometer to quantify total migrated cells. Flow cytometry was used to identify cellular subsets.

ELISA and cytokine arrays. CXCL12 detection in CM was performed using Mouse CXCL12/SDF-1α DuoSet ELISA Kit (R&D) according to manufacturer's instructions. Absorbance was determined at 450 nm on Multiskan GO plate reader (Thermo Fisher Scientific). Cytokine assay was performed using Proteome Profiler Mouse XL Cytokine Array Kit (R&D) according to manufacturer's instruction. The membranes were placed in an autoradiography film cassette and exposed to X-ray film for 2, 5 and 10 min. Data acquisition and quantification was performed using ImageQuant TL V2005 (Amersham Biosciences).

Histology. 5-μm sections of paraffin-embedded pancreatic tissues were analyzed for H&E (Thermo Fisher Scientific), Picro-Sirius Red (Sigma-Aldrich) and Masson's Trichrome (Diagnostic Biosystems) according to manufacturer's instructions.

10×, 20× and 40× images were taken on the Nikon Eclipse 80i bright field microscope (Nikon). Whole-tissue slide scans at 10× magnification were performed on the Nikon Eclipse Ci Slide Scanner (Nikon, Objective Imaging). Image analysis was performed by thresholding for positive staining and normalizing to total tissue area, using ImageJ (NIH) and Metamorph v7.7.0.0 (Molecular Devices) software.

Immunofluorescence. 5-μm-thick sections were air-dried and fixed in 4% PFA (Ted Pella) for 15 min before being washed thrice with PBS. Tissues were permeabilized by incubating the slides in 0.5% Triton X-100 in PBS for 15 min at RT, and peroxidase-quenched by incubating in 1% hydrogen peroxide (Invitrogen) for 10 min at 22 °C (RT). After blocking for 1 h at RT in blocking buffer (5% goat serum, 2.5% BSA in 1× PBS), slides were incubated overnight in a humidified chamber at 4 °C with anti-mouse antibodies listed in **Supplementary Table 2**. Following PBST (1× PBS with 0.05% Tween-20) washes, slides were incubated with Alexa Fluor 594- or Alexa Fluor 647–conjugated goat anti-mouse/rabbit secondary antibody (Molecular Probes). For immunofluorescence staining by Tyramide Signal Amplification (TSA), slides were additionally blocked using an Avidin/Biotin Blocking Kit (Vector Labs) after using blocking buffer. After primary incubation and washes, streptavidin-HRP conjugate (PerkinElmer) was added and incubated for 30 min at RT. After three washes in PBST, slides were incubated with TSA-Biotin (PerkinElmer) for 8 min at RT. After PBST washes, slides were incubated with Streptavidin-Alexa Fluor 594 (Life Technologies) for 30 min. Slides were subsequently washed and mounted using Vectashield w/DAPI (Vector Labs). For cell immunofluorescence staining, 5,000 normal pancreatic fibroblasts were seeded into an 8-well chamber slide (Lab-Tek II; Thermo Fisher Scientific) and cultured overnight. Slides were then processed as described previously for tissue immunofluorescence staining.

10×, 20× and 40× images were taken on the Nikon Eclipse 80i Epifluorescence microscope (Nikon). Whole-tissue slide scans at 10 × magnification were performed on the Nikon Eclipse Ci Slide Scanner (Nikon, Objective Imaging). Image analysis was performed by thresholding for positive staining and normalizing to total tissue area, using ImageJ (NIH) and Metamorph v7.7.0.0 (Molecular Devices) software.

Immunohistochemistry (IHC). Tissues were fixed in 10% formalin, embedded in paraffin, and incubated with antibodies as previously described (5). Briefly, 5-μm-thick sections were deparaffinized in xylene, rehydrated in graded ethanol and subjected to antigen retrieval by steam heating in Citra antigen retrieval solution (BioGenex). After blocking for 1 h at RT in blocking buffer (5% goat serum, 2.5% BSA in 1× PBS), slides were incubated overnight in a humidified chamber at 4 °C with anti-mouse/human antibodies listed in **Supplementary Table 4**. Immunostaining was detected using either 3,3′-diaminobenzidine (DAB) and Ultravision LP detection system (Thermo) or using indirect immunofluorescence. Image acquisition and analysis was similar to that of immunofluorescence imaging, described elsewhere.

Quantitative reverse transcription–polymerase chain reaction. Total RNA was extracted from BM-MACs using an E.Z.N.A. Total RNA Kit (OMEGA). cDNAs were synthesized using qScript cDNA SuperMix (QuantaBio). Quantitative real-time PCR Taqman primer probe sets specific for *Arg1*, *Ym1* and *Ccl2* (Applied Biosystems) were used, and the relative gene expression was determined on an ABI 7900HT quantitative PCR machine (ABI Biosystems) using Taqman Gene Expression Master Mix (Applied Biosystems). The comparative threshold cycle method was used to calculate fold changes in gene expression, which were normalized to the expression of *Tbp* and/or *Gapdh* as reference genes.

Immunoblotting. Briefly, equal amounts of cells were harvested in standard RIPA buffer supplemented with protease and phosphatase inhibitors (Roche). Protein lysates were resolved in Tris/glycine SDS PAGE gels and transferred onto PVDF membranes (Invitrogen). Membranes were blocked with 5% Milk powder in 1× TBS buffer containing 0.05% Triton X-100, and subsequently probed overnight at 4 °C with primary WB antibodies listed in **Supplementary Table 4**. Bands were probed with HRP-conjugated secondary antibodies (Cell Signaling Technology) and visualized using ECL Substrate (Thermo Fisher Scientific) on ChemiDoc XRS+ system (Bio-Rad).

doi:10.1038/nm.4123

Microarray analysis. Microarray was performed by Genome Technology Access Center (GTAC) at Washington University and data generated has been deposited in NCBI's Gene Expression Omnibus with accession number GSE75233. Total RNA from tumor tissues of KP tumor-bearing mice treated with vehicle and FAKi was isolated and subsequently processed for microarray hybridization using Agilent Mouse 8× 60K Expression Microarrays according to the manufacturer's instruction (Agilent Technologies). Raw data were log2-transformed and quantile-normalized across all samples. Detectable genes were defined as those with a detected call in at least 10% of samples studied. R software package *limma* (Bioconductor) was used to detect differentially expressed genes in FAKi-treatment groups with respect to vehicle. Significant genes were determined at $P < 0.05$ and absolute fold-change ≥1.5. Top differentially regulated genes are listed in **Supplementary Table 1**.

Randomization of mouse models to treatment groups. Genetic KPC and KPPC mice were enrolled into treatment groups in an alternating enrolment using birth date and animal number to assign order. All animals were assigned a treatment group by an investigator blinded to their current tumor burden. For both orthotopic and subcutaneous PDAC tumor models, cohorts of mice were randomized into different treatment groups using either gross tumor diameter or tumor volume (length × (width^2)/2). To accomplish randomization, animals were sorted by tumor size in ascending order and then groups were assigned in descending order. Each group was checked *post hoc* to verify no statistical difference in average starting tumor size.

Statistical analyses. All statistical analysis was run using the GraphPad Prism 6.0 software (GraphPad). Sample size for all *in vivo* experiments was determined using experimental data from other studies to approximate number of mice necessary to give >85% confidence for a twofold change in any given parameter at the $P < 0.05$ significance level. The number of animals and replicate *in vitro* experiments is specified in each figure legend. The majority of the data presented have normal distribution and similar variance. However, variance was first systematically examined using an *F*-test, and Mann–Whitney *U*-test or Student's *t*-test employed accordingly. Kaplan–Meier survival curves were calculated using the survival time for each mouse from all treatment groups, and significance was determined by log-rank test. For tumor burden analyses and image quantifications, statistical significance was assayed by Student's *t*-test or one-way ANOVA. Significance of metastases' frequency was determined by Fisher's exact test. $^*P < 0.05$; $^{**}P < 0.01$; n.s. denotes not significant. All data are presented as mean ± s.e.m. or as box plots.

54. Kim, M.P. *et al.* Generation of orthotopic and heterotopic human pancreatic cancer xenografts in immunodeficient mice. *Nat. Protoc.* **4**, 1670–1680 (2009).
55. Weischenfeldt, J. & Porse, B. Bone marrow–derived macrophages (bmm): isolation and applications. *Cold Spring Harb. Protoc.* **12**, pdb-prot5080 (2008).
56. Pelham, R.J. Jr. & Wang, YI. Cell locomotion and focal adhesions are regulated by substrate flexibility. *Proc. Natl. Acad. Sci. USA* **94**, 13661–13665 (1997).